function, but it also appeared useful as an important predictor for postoperative outcome. Normal findings on renography meant no contraindication to heart transplantation and good conditions for immunosuppressive therapy. Pathological findings on renograms, as seen in Groups II and III, indicated a high probability of postoperative renal dysfunction, possibly a contraindication to heart transplantation. The more severe the abnormal changes on pretransplant renography, the more they represented important signs heralding risk for the heart transplantation itself, predicting a stormy postoperative course. We now consider these abnormal changes to be a relative contraindication to heart transplantation. Renal scintigraphy provided a simple and economical method for functional evaluation, giving information that can readily be combined with anatomic renal parameters, as demonstrated by CT, ultrasound or MRI, if necessary.

## REFERENCES


1. Primo G, Le-Clerc JL, Antoine M, De-Smet JM, Joris M. A survey of nine years heart transplantation at Erasme Hospital, University of Brussels. *Acta Cardiol* 1991;46:555–565.
2. Livi U, Milano A, Bortolotti U, Casula R, Zenati M, Casarotto D. Results of heart transplantation by extending recipient selection criteria. *J Cardiovasc Surg (Torino)* 1994;35:377–382.
3. Oppenheim BE, Appledorn CR. Parameters for functional renal imaging. In: Esser PD. *Functional mapping of organ systems and other computer topics*. New York: The Society of Nuclear Medicine; 1981:39–55.
4. Nicoletti R. A program for fully automatic processing of dynamic kidney studies. *UGS Newsletter* 1986;3:14–16.
5. Valentinuzzi ME, Montaldo E, Volachec M. Discrete deconvolution. *Med Biol Engl Comput* 1975;13:123–125.
6. Diffey BL, Corfield JR. Data-bounding technique in discrete deconvolution. *Med Biol Engl Comput* 1976;14:478.
7. Thurau K. Kontrolle des glomerulumfiltrats durch den tubulo-glomerulären rückkoppelungs-mechanismus und seine beeinflussung durch furosemid. *Nieren Hochdruckkrankheiten* 1985;6:221–223.
8. Kyo S, Omoto R. Indication and clinical results of heart transplantation in the terminal stage of ischemic cardiomyopathy. *Nippon Geka Gakkai Zasshi* 1996;97:240–244.
9. Brodaty D, de-Lentdecker P, Dubois C, et al. Long-term results of cardiac transplantation. *Arch Mal Coeur Vaiss* 1995;88:981–986.
10. Loisance D, Mazzucotelli JP, Benvenuti C, et al. Cardiac transplantation: results after 5 years. *Arch Mal Coeur Vaiss* 1995;88:1273–1276.
11. Sander M, Victor RG. Hypertension after cardiac transplantation: pathophysiology and management. *Curr Opin Nephrol Hypertens* 1995;4:443–451.
12. McGiffin D, Tauxe WN, Lewis C, Karp R, Mantle J. The relationship between cardiac output and effective renal plasma flow in patients with cardiac disease. *Eur J Nucl Med* 1984;9:542–544.
13. Tauxe WN, Dubovsky EV, Mantle JA, Dustan HP, Logic JR. Measurement of effective renal plasma flow in congestive heart failure. *Eur J Nucl Med* 1981;6:555–559.
14. Flückiger F, Fueger GF, Hausegger K, Nicoletti R. Results of quantification of frusemide response in 123-I-hippuran renal studies of unilateral renal artery stenosis in. In: Blaufox MD, Hollenberg NK, Raynaud C, eds. *Radionuclides in nephro-urology*, Contributions in nephrology. Basel: Karger Verlag; 1990:196–199.
15. Britton KE, Nimmon CC, Whitfield HN, Kelsey-Fry I, Hendry WG, Wickham JEA. The evaluation of obstructive nephropathy by means of parenchymal retention. In: Hollenberg NK, Lange S, eds. *Proceedings of the fourth international symposium on radionuclides in nephrology*. Stuttgart, Germany: Georg Thieme; 1980:164–172.
16. Bischof-Delaloye A, Wauters JP, Delaloye B. 123-I-hippuran renography: accumulation and elimination indices in the long-term follow-up of renal transplants. In: Joekes AM et al., eds. *Radionuclides in nephrology*. London: Academic Press; 1982:284–294.
17. Thomsen HS, Bartram P, Hvid-Jacobsen K, Nielsen SL. Prospective evaluation of radionuclide monitoring in renal transplantation. In: Blaufox MD, Hollenberg NK, Raynaud C, eds. *Radionuclides in nephro-urology, Contributions in nephrology*. Basel: Karger Verlag; 1990:108–112.
18. Magnusson G, Lewander R, Lundgren G, Sarby B, Svensson L, Thornström S. The intrarenal kinetics of hippuran in acute rejection of renal allograft. In: Blaufox MD, Hollenberg NK, Raynaud C, eds. *Radionuclides in nephrourology*, Contributions in nephrology. Basel: Karger Verlag; 1990:123–126.
19. Magnusson G, Groth CG, Lewander R, et al. Ischemic injury to renal allografts studied by gamma camera technique using 123-I-hippuran. In: *Proceedings sixth international symposium on radionuclides in nephrology*. Basel: Karger Verlag; 1987:178–185.
20. Li Y, Russell CD, Palmer-Lawrence J, Dubovsky EV. Quantitation of renal parenchymal retention of technetium-99m-MAG3 in renal transplants. *J Nucl Med* 1994;35:846–850.
21. Makoba GI, Nimmon CC, Kouykin V, Gupta AK, Gupta H, Britton K. Comparison of a corticopelvic transfer index with renal transit times. *Nucl Med Commun* 1996;17:212–215.
22. Wenger NK, Goodwin JF, Roberts WC. Cardiomyopathy and myocardial involvement in systemic disease. In: Hurst JW, Logue RB, Schlant RC, Sonnenblick EH, Wallace AG, Wenger NK, eds. *The heart*, vol. 58. New York: McGraw-Hill; 1996:1181–1248.
23. Dzau VJ. Renal and circulatory mechanism in congestive heart failure. *Kidney Int* 1987;31:1402–1415.
24. Hamer J. Therapeutic aspects of heart failure. *Curr Opin Cardiol* 1986;1:354–369.


# Post-Therapy Iodine-131 Localization in Unsuspected Large Renal Cyst: Possible Mechanisms


Christopher Wen, Elaine Iuanow, Elizabeth Oates, Stephanie L. Lee and Ronald Perrone

*Departments of Radiology and Internal Medicine, New England Medical Center and Tufts University School of Medicine, Boston, Massachusetts*



Sensitive and specific, whole-body $^{131}$I scintigraphy remains an important technique for diagnosing metastases from differentiated papillary or follicular thyroid carcinoma. False-positive $^{131}$I localization is well recognized and can occur in a variety of conditions. We present a case of intense $^{131}$I localization in a previously unsuspected large renal cyst; the lesion was not visualized on routine preablation diagnostic $^{131}$I scintigraphy but was obvious on post-therapeutic whole-body imaging, underscoring the value of post-therapy imaging in detecting abnormalities not apparent on diagnostic studies. Radioiodine within the urinary bladder or, at times, the renal collecting system is expected, because $^{131}$I excretion is primarily by glomerular filtration. In the case presented here, $^{131}$I activity within the renal cyst supports the concept that iodide is subject to an active secretory process by the renal tubule.



**Key Words:** thyroid carcinoma; iodine-131; renal cyst

**J Nucl Med 1998; 39:2158–2161**


Whole-body $^{131}$I scintigraphy and monitoring of thyroglobulin levels remain the mainstays for follow-up of patients with well-differentiated papillary or follicular thyroid cancer. False-positive $^{131}$I localization on diagnostic scans has been well documented (*1–9*); it is important to recognize false-positive sites to avoid unnecessary ablation therapy. Radioiodine localization in a renal cyst during diagnostic $^{131}$I imaging has been described (*1*). We report marked radioiodine activity in an unknown large renal cyst visualized only on the postablation $^{131}$I scan.


Received Dec. 3, 1997; revision accepted Apr. 19, 1998.



For correspondence contact: Elizabeth Oates, MD, Division of Nuclear Medicine, Department of Radiology, New England Medical Center, 750 Washington St., NEMC #228, Boston, MA 02111. No reprints available.

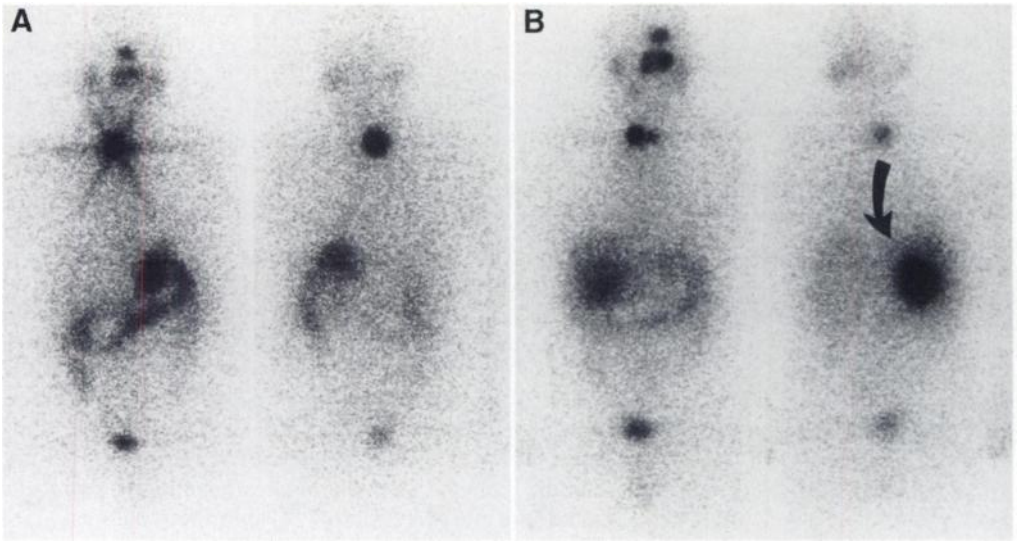


**FIGURE 1.** (A) Diagnostic $^{131}$I whole-body scan. Anterior (left) and posterior (right) views 48 after ingestion of 2.9 mCi demonstrate thyroid bed remnant and normal bowel. Subtle $^{131}$I localization is seen in region of right upper kidney. (B) Therapeutic $^{131}$I whole-body scan. Anterior (left) and posterior (right) views 6 days after ablation with 150 mCi demonstrate intense focal $^{131}$I localization in posterior right upper abdomen (arrow).

## CASE REPORT

The patient is a 53-yr-old man who presented with a palpable mass on the left side of his neck during routine physical examination. There were no associated symptoms and no history of irradiation to the head or neck. CT delineated a 2.2 × 1.8 × 5.0 cm, nonenhancing cystic mass in the left neck posterior to the carotid sheath and sternocleidomastoid muscle. A biopsy of the mass was performed; histopathology revealed metastatic papillary thyroid carcinoma. The patient underwent subtotal thyroidectomy and left supraomohyoid neck dissection; surgical pathology disclosed a 0.6-cm papillary thyroid carcinoma in the left thyroid lobe, with microscopic invasion through the surgical margin and two metastatic lymph nodes in the left neck. The patient tolerated the surgery well and was started on L-thyroxine. At 3 mo postsurgery, the patient returned in a hypothyroid state for diagnostic (3 mCi) $^{131}$I whole-body scintigraphy (Fig. 1A). The scan showed uptake in only the thyroid bed consistent with remnant thyroid tissue and no local or distant disease.

Because of an elevated thyroglobulin level of 48.9 ng/ml off hormone, regional lymph node metastases and positive surgical margins, the patient was admitted for therapeutic (150 mCi) $^{131}$I. Six days later, repeat whole-body imaging (Fig. 1B) showed not only the expected uptake in the residual thyroid bed, but, surprisingly, a large, round focus of $^{131}$I activity in the posterior right upper abdomen. Adjunctive SPECT imaging localized this abnormality posterior and inferior to the liver in the region of the right upper kidney. Same-day, $^{99m}$Tc-diethylenetriamine pentaacetic acid (DTPA) 30-min, dynamic renal imaging (Fig. 2) was performed using a high-energy collimator with the gamma camera peaked for $^{99m}$Tc. The high photon flux of $^{99m}$Tc overwhelmed the relatively low $^{131}$I counts, thus avoiding significant downscatter and septal penetration. Renal imaging demonstrated an avascular, well-circumscribed, cold lesion in the upper pole of the right kidney corresponding to the focal $^{131}$I localization. Renal uptake and excretion were nearly symmetric, implying that the glomerular filtration rate was not affected significantly by the cyst. The skin overlying the $^{131}$I radioactivity was marked for correlation with same-day ultrasonography (Fig. 3), which showed a large, round, well-defined anechoic cyst involving the upper pole of the right kidney.

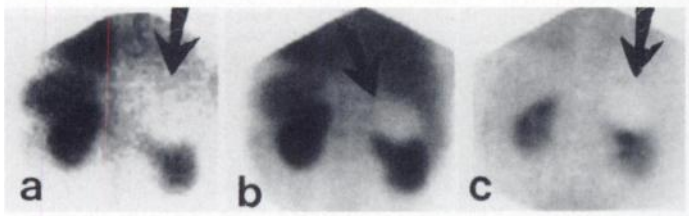


**FIGURE 2.** Renal scan. Selected images at 1 (A), 12 (B) and 31 min (C) after intravenous injection of 25 mCi $^{99m}$Tc-DTPA demonstrate large, well-defined, avascular, nonfunctional mass arising from upper pole of right kidney (arrows). Slight inferior displacement of right kidney from mass effect without urinary obstruction is seen as collecting system activity cleared over time.

One year later, repeat diagnostic $^{131}$I (3 mCi) scintigraphy showed complete ablation of the thyroid remnant and no $^{131}$I-avid metastases. Delayed imaging at 6 days showed faint activity in the now-known renal cyst. Nine and 15 mo post-therapy, thyroglobulin levels on hormone replacement remained low (1.7 and 0.5 ng/ml, respectively). Follow-up renal ultrasonography at 15 mo showed no change in the appearance or size of the renal cyst.

## DISCUSSION

False-positive radioiodine localization has been well documented and can be broadly classified into general categories (Table 1) (*1–9*). One report described false-positive uptake in a renal cyst on diagnostic $^{131}$I imaging (*1*). The case presented here is unusual in that an unsuspected large renal cyst was not visualized on the initial diagnostic image but appeared intense on postablation images. In a series of 39 patients, new findings or better delineation of equivocal findings were demonstrated in half on post-therapeutic scintigraphy (*10*), thus underscoring the value of immediate follow-up imaging.

Possible mechanisms to explain our observation include the

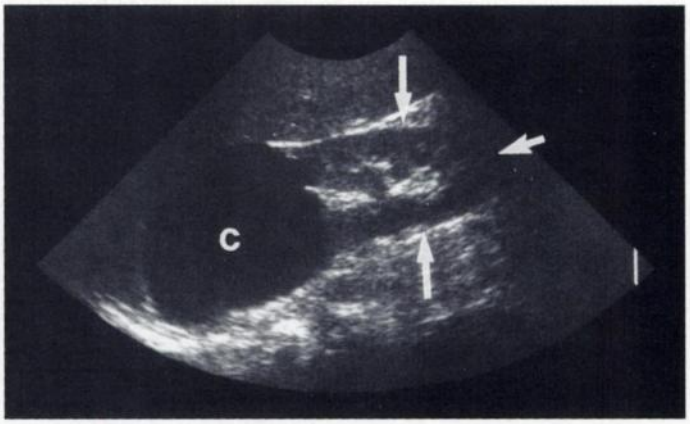


**FIGURE 3.** Right renal longitudinal sonogram demonstrates 7.5 × 8.6 × 8.7 cm round, anechoic structure at upper pole that has features characteristic of benign simple cyst (c). Normal kidney (arrows).

**TABLE 1**
Sources of False-Positive Radioiodine Localization

| Mechanism | Etiology |
|---|---|
| Physiologic | Urine, sweat, breasts, nasopharynx, respiratory secretions, saliva or salivary glands, vomitus, stomach, large and small intestines, liver, kidneys, bladder, sebaceous cysts |
| Pathologic nonthyroidal conditions | Chronic cholecystitis, periodontal disease, dacrocystitis, thymus, gallbladder, hiatal hernia, Meckel's diverticulum, thyroglossal duct, ectopic kidney |
| Tumors | Lung, ovarian, stomach, meningioma, Warthin's tumor |
| Foreign body contamination | Artificial eye, handkerchief nose ring, hair |

enormous volume of the cyst, a higher plasma $^{131}$I level (50 times higher than usual), longer time interval between dosing and imaging (6 days versus 48 hr) and improved target-to-background ratio. Higher doses result in greater spatial resolution over lower-dose diagnostic scans. In addition, high iodide retention caused by extreme hypothyroidism and low-iodine diet (preparation for scanning and subsequent ablative therapy) probably potentiated cyst visualization. Of related interest, transient enhancement and increased attenuation of renal cysts have been observed on delayed CT scanning after administration of iodinated contrast media; mechanisms proposed for iodine entry into these cysts include communication with the collecting system and diffusion from renal sinus lymphatics (*11,12*).

In this patient, the avascular, nonfunctional nature of the renal cyst on DTPA imaging suggests that the iodide activity entered and remained primarily by active secretion. To support this hypothesis, regions of interest on anterior (heart) and posterior (kidney cyst) views were drawn, counts determined (background = liver and nonbowel abdominal activity) and counts per pixel calculated. Cyst counts (14.7 counts/pixel) exceeded those of the heart (3.6 counts/pixel) by approximately fourfold. Considering that free $^{131}$I was present in plasma only during the initial period after administration and that most of the unexcreted plasma activity detected on Day 6 was likely to be protein-bound, the true ratio of cyst activity to plasma activity is likely to be substantially greater. The magnitude of the difference is readily appreciated visually on this heavily windowed, low-count-rate study (Fig. 1B). Also, the patient's hypothyroid state probably reduced the glomerular filtration rate, making the overall contribution from filtration seem negligible.

Renal cysts can be idiopathic (simple), hereditary or acquired. Renal cysts in autosomal dominant polycystic kidney disease (ADPKD) develop from renal tubule segments caused by abnormal cellular proliferation, accumulation of intratubular liquid as a result of active transepithelial secretion and remodeling of the extracellular matrix (*13*). The origin of simple renal cysts is not well characterized but probably involves similar mechanisms to ADPKD but limited to only a small number of tubules. When small, ADPKD cysts communicate with nephrons, but as they grow, connections with parent tubules are lost, and the cysts become isolated sacs (*14*). Cyst epithelia, despite abnormal growth patterns, exhibit secretory activity and resemble tubular epithelium (*14*). Iodide behaves similarly to chloride and is freely filtered at the glomerulus. Tubular epithelial secretion operates through a sodium–potassium adenosinetriphosphatase pump located on the basolateral surface. This pump maintains a low intracellular sodium concentration, which drives an electrically neutral Na/K/2Cl cotransporter also located on the basolateral surface. A cystic fibrosis transmembrane regulator (CFTR) chloride channel on the apical surface of the epithelium is activated by cyclic adenosine monophosphate to secrete chloride ions into the lumen. The CFTR chloride channel, whose diminished function leads to thickened secretions and malabsorption in cystic fibrosis, is thought to function in the renal cysts of ADPKD in secreting chloride ions (*15*). It is thus postulated that iodide enters the basolateral aspect of the cell through the electrically neutral Na/K/2Cl cotransporter and exits the cell through the apical CFTR channel. These mechanisms probably mediate the active transcellular secretion of iodide into the cyst lumen. The recently cloned human sodium iodide symporter (hNIS) has been localized to the thyroid, colon, breast and ovaries but was not detected in the kidneys (*16*). Therefore, it is unlikely that hNIS is responsible for the secretion of $^{131}$I into the renal cyst.

At follow-up, the patient's low thyroglobulin level supported no residual disease (*17*). The vast majority of distant thyroid carcinoma metastases involve the lungs, bone and mediastinum. A minority of metastases are found elsewhere, half are in the brain, a quarter in the liver and the rest in other locations. Thus, metastatic disease to a renal cyst would be distinctly unusual. If this cyst were a metastasis, the thyroglobulin level would be expected to be elevated, and other metastases would be likely. In addition, renal cysts are common in the general population but tend to be smaller than the one encountered in this patient. Conversely, thyroid cancer is relatively uncommon. On routine or even post-therapeutic radioiodine imaging, visualization of small renal cysts would not be expected given their relatively minimal $^{131}$I concentration and resolution limitations.

This article supports the value of post-therapy whole-body $^{131}$I imaging in detecting abnormalities not apparent on the diagnostic scan because of higher plasma concentration, improved target-to-background ratio and more time between dosing and imaging. The underlying pathophysiology can be linked to the hypothesized active iodide secretory mechanism into renal cysts involving the CFTR apical transporter present in normal renal tubular epithelium and adult polycystic kidney disease cysts.

## ACKNOWLEDGMENTS

The authors thank Richard Behrman, medical physicist, and Jeffrey L. Becker, chief nuclear medicine technologist, New England Medical Center, for their assistance with calculations used in this article.

## REFERENCES

1. Brachman MB, Rothman BJ, Ramanna L, Tanasescu DE, Adelberg H, Waxman AD. False-positive iodine-131 body scan caused by a large renal cyst. *Clin Nucl Med* 1988;13:416–418.
2. Bakheet SM, Hammami MM, Powe J. False-positive radioiodine uptake in the abdomen and the pelvis: radioiodine retention in the kidneys and review of the literature. *Clin Nucl Med* 1996;21:932–937.
3. Sutter CW, Masilungen BG, Stadalnik RC. False-positive results of I-131 whole-body scans in patients with thyroid cancer. *Semin Nucl Med* 1995;25:279–282.
4. Brucker-Davis F, Reynold JC, Skarulis MC, et al. False-positive iodine-131 whole-body scans due to cholecystitis and sebaceous cyst. *J Nucl Med* 1996;37:1690–1693.
5. McDougall IR. Whole-body scintigraphy with radioiodine-131: a comprehensive list of false-positives with some examples. *Clin Nucl Med* 1995;20:869–875.
6. Bakheet SM, Hammami MM. False-positive radioiodine whole-body scan in thyroid cancer patients due to unrelated pathology. *Clin Nucl Med* 1994;19:325–329.
7. Salvatori M, Saletnich I, Rufini V, Troncone L. Unusual false-positive radioiodine whole-body scans in patients with differentiated thyroid carcinoma. *Clin Nucl Med* 1997;22:380–384.
8. Greenler DP, Klein HA. The scope of false-positive I-131 images for thyroid carcinoma. *Clin Nucl Med* 1989;14:111–117.
9. Achong DM, Oates E, Lee SL, Doherty FJ. Gallbladder visualization during post-therapy iodine-131 imaging of thyroid carcinoma. *J Nucl Med* 1991;32:2275–2277.

10. Spies WG, Wojtowicz CH, Spies SM, Shah AY, Zimmer AM. Value of post-therapy whole-body I-131 imaging in the evaluation of patients with thyroid carcinoma having undergone high-dose I-131 therapy. *Clin Nucl Med* 1989;14: 793–800.
11. Shanser JD, Hedgcock MW, Korobkin M. Transit of contrast material into renal cysts following urography or arteriography [Abstract]. *AJR* 1978;130:584.
12. Mayer DP, Baron RL, Pollack HM. Increase in CT attenuation values of parapelvic cysts after retrograde pyelography. *AJR* 1982;139:991–993.
13. Grantham JJ. Fluid secretion, cellular proliferation, and the pathogenesis of renal epithelial cysts. *J Am Soc Nephrol* 1993;3:1843–1857.
14. Gardner KD, Glew RH, Evan AP, McAteer JA, Bernstein J. Why renal cysts grow. *Am J Physiol* 1994;266:F353–F359.
15. Sullivan LP, Wallace DP, Grantham JJ. Chloride and fluid secretion in polycystic kidney disease. *J Am Soc Nephrol* 1998;9:903–916.
16. Smanik PA, Ryu KY, Theil KS, Mazzaferri EL, Jhiang SM. Expression, exonintron organization, and chromosome mapping of the human sodium iodide symporter. *Endocrinology* 1997;138:3555–3558.
17. Ozata M, Suzuki S, Miyamoto T, Liu RT, Fierro-Renoy R, DeGroot LJ. Serum thyroglobulin in the follow-up of patients with treated differentiated thyroid cancer. *J Clin Endocrinol Metab* 1994;79:98–105.

# Biodistribution and Kinetics of Holmium-166-Chitosan Complex (DW-166HC) in Rats and Mice

Yuka S. Suzuki, Yuko Momose, Noriko Higashi, Akiyo Shigematsu, Kyung-Bae Park, Young Mi Kim, Jae Rok Kim and Jei Man Ryu

*Institute of Whole Body Metabolism, Chiba, Japan; Department of Radioisotopes, Korea Atomic Energy Research Institute, Taejon, Korea; and Research Laboratory, Dong Wha Pharmaceutical Company, Kyunggi-do, Korea*

The fate of $^{166}$Ho-chitosan complex, a radiopharmaceutical drug for cancer therapy, was determined by studying its absorption, distribution and excretion in rats and mice. **Methods:** Holmium-166-chitosan complex [0.75 mg of $Ho(NO_3)_3 \cdot 5H_2O$ and 1 mg chitosan/head] was administered intrahepatically to male rats. Radioactive concentrations in blood, urinary and fecal excretion and radioactive distribution in tissues were examined. To determine the effects of chitosan in $^{166}$Ho-chitosan complex, $^{166}$Ho alone [0.75 mg of $Ho(NO_3)_3 \cdot 5H_2O$/head] was intrahepatically administered to male rats, and radioactive concentrations in blood, urinary and fecal excretion and radioactive distribution were examined. In B16 melanoma-transplanted nude mice, radioactive distribution after intratumoral administration of $^{166}$Ho-chitosan complex [0.075 mg of $Ho(NO_3)_3 \cdot 5H_2O$ and 0.10 mg chitosan/head] was investigated also. **Results:** After administration of $^{166}$Ho-chitosan complex, the radioactive concentrations in blood were low, and cumulative urinary and fecal excretions over a period of 0–72 hr were 0.53% and 0.54%, respectively. The radioactive concentrations in tissues and the whole-body autoradiography images showed that most of the administered radioactivity was localized at the administration site, and only slight radioactivity was detected from the liver, spleen, lungs and bones. On the other hand, results of intrahepatic administration of $^{166}$Ho alone showed high radioactive concentrations in the blood, and the whole-body autoradiographs showed that the administered radioactivity was distributed in many organs and tissues. These results strongly suggest that $^{166}$Ho is retained at the administration site only when it forms a chelate complex with chitosan. Autoradiographs after intratumoral administration of $^{166}$Ho-chitosan complex showed that radioactivity was localized at the site of administration without distribution to the other organs and tissues. **Conclusion:** Administered $^{166}$Ho-chitosan complex is retained at the administration site after either intrahepatic or intratumoral administration to rats or tumor-transplanted nude mice.

**Key Words:** internal radiotherapy; liver cancer; radiopharmaceutical drug

**J Nucl Med 1998; 39:2161–2166**

There are several articles showing biodistribution after the administration of internal radiotherapeutic agents (*1–4*). These studies are focused on obtaining higher concentrations of the radioactivity and longer retention times in the tumor compared with normal tissues to show the therapeutic effects with high selectivity and to avoid radiation damage to normal tissue or organs. Many antibodies against tumors have been studied (*5–7*), and their selectivities to the tumor cells allow intravenous injection. The other approach uses a radionuclide-bound resin that is physically trapped in the blood vessels of the target tumor (*4,8–12*).

Holmium-166-chitosan complex (DW-166HC), in which chitosan is chelated with 166-holmium, is being developed as a radiopharmaceutical drug for cancer therapy by the Korea Atomic Energy Research Institute (Taejon, Korea) and Dong Wha Pharmaceutical Company (Kyunggi-do, Korea). Chitosan, a polymer of 2-deoxy-2-amino-D-glucose that is obtained by deacetylation of chitin, forms a chelate with the heavy metals (*13–15*). It is readily dissolved in water to make a clear solution under acidic conditions, but it converts to a solid state under basic conditions. Holmium-166 has many beneficial physical characteristics for internal radiation therapy, such as an appropriate half-life (26.8 hr), high beta-energy [maximum 1.85 MeV (51%), 1.77 MeV (48%); mean = 0.67 MeV) and low gamma-energy (0.081 MeV) that is easily detectable by gamma camera. Direct administration of DW-166HC in acidic solution into the lesion of the tissue percutaneously converts the solution to a gel in the tissue, and radioactivity of $^{166}$Ho destroys the tumor.

When DW-166HC is applied for clinical therapy, the pharmacokinetic profile gives important information on both therapeutic efficacy and side effects. The objective of this study, therefore, is to determine the fate of DW-166HC by studying its absorption, distribution and excretion after intrahepatic, intravenous and intratumoral administration to male rats and nude mice.

## MATERIALS AND METHODS

### Chemicals

Holmium-166-$(NO_3)_3 \cdot 5H_2O$ was produced at the Korea Atomic Energy Research Institute. Specific activities of $^{166}Ho(NO_3)_3 \cdot 5H_20$ were between 65 and 296 MBq/mg (1.75 and 8.0 mCi/mg). Chitosan was obtained from Korea CCR (Seoul, Korea), and its molecular weight was ~700,000. All other chem-

Received Oct. 1, 1997; revision accepted Mar. 2, 1998.
For correspondence or reprints contact: Yuka S. Suzuki, PhD, 340-2 Nauchi, Shiroi, Inba, Chiba, 270-14 Japan.